Lotte Scheder-Bieschin, Tom Van Mele, Philippe Block

Curved-Crease Flat-Foldable Bending-Active Plate Structures

Abstract: Curved-crease folded (CCF) bending-active plates efficiently form complex curvilinear geometries with structural applications. Instead, this research proposes joining stacked plates along common curved creases into flat-foldable configurations. These unfold with an accordion-like one-degree-of-freedom mechanism into corrugated spatial structures. The proposed system, termed curved-crease unfolding (CCU), allows for simple 2D prefabrication, flat-packed transport, and rapid on-site deployment. Its globally double-curved and articulated structural geometry extends the design space of CCF and finds application as structure and formwork. This research translates the fundamental geometric design principles of CCF to CCU for planar creases and demonstrates the design space for a multi-crease corrugated structure with non-zero thickness. A parametric model is implemented for the geometric construction and kinematic deployment in the COMPAS framework. Its deployment is validated by capturing the mechanical behavior with finite element simulation in the software SOFiSTiK. The paper demonstrates the non-developability conditions for convex synclastic and concave anticlastic creases. For the special cases of planar creases, angle correlations are formulated with direct inversion from CCF using discrete differential geometry. The trigonometric correlation for the kinematic deployment is applied to the discrete mesh representation. Inclining subsequent osculating planes reveal restricted geometric applicability regarding crease planarity. The non-zero thickness is modeled with an axis-shift approach. Finally, a rule catalog for global shape control is derived based on crease profiles and plane layouts with inclinations resulting in synclastic and anticlastic multi-crease designs. These would be challenging to construct otherwise and are enabled solely based on its formation principles.

Keywords: curved-crease folding, flat-foldable unfolding, bending-active plates, non-zero thickness, corrugated structures, discrete geometric modeling, deployment simulation, FE simulation, COMPAS.

1 Introduction

Active bending of plates allows for the efficient formation of lightweight, curvilinear structures without formwork. However, single bending-active plates under external loading deform dramatically and risk stability failure. Their performance improves significantly when mutually restrained along curved creases (Scheder-Bieschin et al. 2022). Thus, curved-crease folded bending-active plates find structural applications
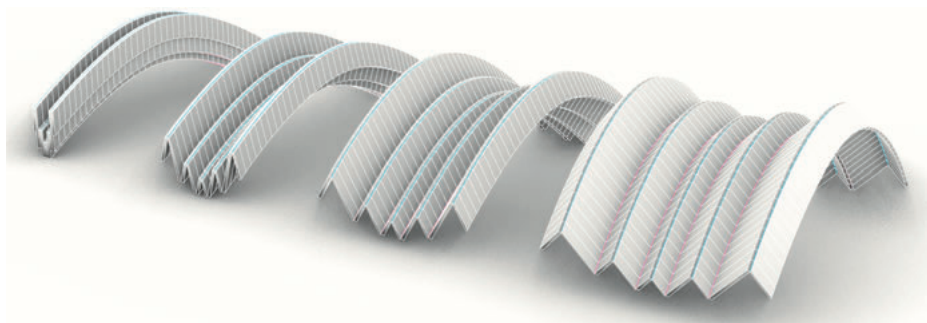
Fig. 1: Deployment of the CCU system from its closed flat-folded configuration to spatial unfolded configuration.

and, moreover, possess complex geometries (Maleczek et al. 2020). Due to plate thicknesses beyond foldability and limited panel size, separate plates are assembled with curved hinges and folded from a flat configuration.

When plate joining is necessary anyhow, stacked plates can be joined along common curved creases into a flat-folded configuration which is then unfolded. In accordance with curved-crease folding (CCF), this research introduces the terminology of curved-crease unfolding (CCU). A non-developable CCU system of multiple flat-folded developable plates unfolds with an accordion-like one-degree-of-freedom mechanism into a corrugated spatial structure of global double curvature (Fig. 1). CCU is compactly flat-packable for transport and can be rapidly deployed on-site into a material-efficient system of structural geometry, which expands the constrained design possibilities of CCF.

The objective of this research is to translate the fundamental geometric design principles of CCF to CCU for a single planar crease system, considering non-zero plate thickness. It aims to demonstrate the design space and associated rules of CCU for a multi-crease corrugated structure validated through finite element (FE) simulation.

2 Background

The feasibility of CCU was demonstrated as a proof-of-concept as formwork for corrugated concrete shells (Scheder-Bieschin et al. 2022). Furthermore, CCU can be identified combined with CCF in closed cross-sections as a single module in a timber bridge (Rihaczek et al. 2022) or array in computational vault explorations (Tachi 2013). The proposed system essentially resembles the vault's horizontally-cut half, avoiding joining more than two creases for fabricability.

Tachi (2013) explicitly introduced the concept of closed-folding based on four quadrants, however, without thickness. Shimoda et al. (2020) demonstrated an axis-

shift approach with uniform thickness panels on a flat-foldable rigid-origami system with a one-directional mechanism termed 'bellow-type'. This essentially equals the proposed bending-active CCU system with the difference that the polygonal creases are more densely discretized for the curved creases and that the discrete transversal hinges of rigid panels are replaced by dense ruling lines of the bending-active strips. Consequently, the ruling direction can readjust increasing design freedom (Sec. 5.1), and the thickness approach considers continuous strain (Sec. 5.3).

3 Methods

This research approaches the geometric design of CCU in comparison to CCF using discrete differential geometry and plate thickness. It focuses on translating the geometric formation principles explicitly, hence, without employing dynamic relaxation or optimization approaches. Angle conditions are formulated for the non-developable CCU versus their developable CCF counterpart. As the paper focuses on planar creases, the design rules for the ruling layout are derived for the special case. For the kinematic modeling of the deployment mechanism, we apply trigonometric correlations in the discretized mesh representation and show implications for the behavior of subsequent creases for a multi-crease corrugated structure. The non-zero thickness is handled with an axis-shift approach. By exploring variations in crease profile and plane layouts with inclinations, a rule catalog is derived for global shape control into doubly-curved designs, revealing the design space.

The computational modeling is implemented in COMPAS, an open-source Python-based framework for research in AEC (Van Mele et al. 2022). As curved-crease unfolded structures are composed of developable strips – cylindrical, conical, or tangent surfaces – which are isometric to a planar configuration, they are discretely represented in a half-edge mesh data structure with quadrilateral planar faces. Beyond the geometric construction in a parametric design model for CCF and CCU, the simulation comprises their geometric deployment and an interface for structural verification.

The simulation with the FE software SOFiSTiK (SOFiSTiK AG 2022) captures the mechanical behavior with bending resistance and potential instabilities. The plates are modeled as QUAD shell elements with plywood of 8 mm thickness on a scale of 2.5 m and with a hinge condition along the curved creases. The plates are actuated by initial pre-bending to avoid buckling and then by crease-alignedinwards forces and perpendicular outwards forces to simultaneously cause plate bending and unfolding. The forces are applied in an iterative procedure with third-order analysis.

4 Fundamental design rules for a single curved crease

4.1 Geometric principle of CCF and CCU

The geometric principle of CCF and CCU is demonstrated using the concept of four quadrants (Fig. 2 top) introduced by Tachi (2013) for the special case of a planar crease that lies within a single osculating plane, allowing for mirror reflection (Sec. 4.2). Reflecting a single plate and its continuation results in four plates encompassing four quadrants. Quadrants Q1 and Q3 are generated by CCF by folding a continuous developable plate, with Q1 folding leftwards and Q3 folding rightwards. Their crease curve (in green) is convex for one plate and concave for the other. Quadrants Q2 and Q4 are generated by CCU by unfolding two mirror-reflected sheets joined along their shared crease. Q2's crease curve is convex for both plates (in blue), while Q4's crease curve is concave for both plates (in pink). Thus, CCU introduces two new types of creases. In a single curved crease with inflection points, the types transition from Q2 to Q4 from its convex to its concave curvature (Fig. 4 middle-left).

T, **N**, and **B** denote the tangent, normal, and binormal vectors in the orthonormal Frenet-Serret frame of the crease curve, while **B** is also the normal of the osculating plane **O**. Let α denote the reflection angle between the crease normal vector **N** and the surface tangent vector **S**, which lies in the **NB**-plane. $\alpha > 0$ for the actuated folded (CCF) and unfolded (CCU) 3D configurations, and $\alpha = 0$ for the unfolded (CCF) and closed-folded flat (CCU) 2D crease patterns. For CCF, the folding angle is $\pi - 2\alpha$, while for CCU, the folding angle is directly 2α (Fig. 2).

The developability conditions of the four quadrants are demonstrated on a single vertex in Fig. 3 with the sector angles denoted by $\beta_{0...3}$, counterclockwise, between the crease curve edges **C** and ruling vectors **R**. The sum of sector angles $\sum_{i=0}^{3} \beta_i = 2\pi$ for Q1 and Q3, indicating their assemblies are developable; $\sum_{i=0}^{3} \beta_i < 2\pi$ for Q2, indicating its assembly is synclastic; and $\sum_{i=0}^{3} \beta_i > 2\pi$ for Q4, indicating its assembly is anticlastic, despite the plates being monoclastic.

For a planar crease, in Q2 and Q4, the neighboring sector angles on the adjacent plate are equal, $\beta_0 = \beta_3$ and $\beta_1 = \beta_2$. Consequently, the sums of both sector angles on each side are equal, $\sum_{i=0}^{1} \beta_i = \sum_{j=2}^{3} \beta_j$ and $< \pi$ for the convex crease in the synclastic Q2 and $> \pi$ for the concave crease in the anticlastic Q4. However, this sector angles correlation cannot apply for the developable Q1 and Q3, as $\sum_{i=0}^{1} \beta_i < \pi \neq \sum_{j=2}^{3} \beta_j > \pi$ for the convex – and concave crease side, respectively. However, a crossover correlation exists for the ruling angle γ between the ruling **R** and tangent **T**, quantified depending on the special cases (Sec. 4.2).
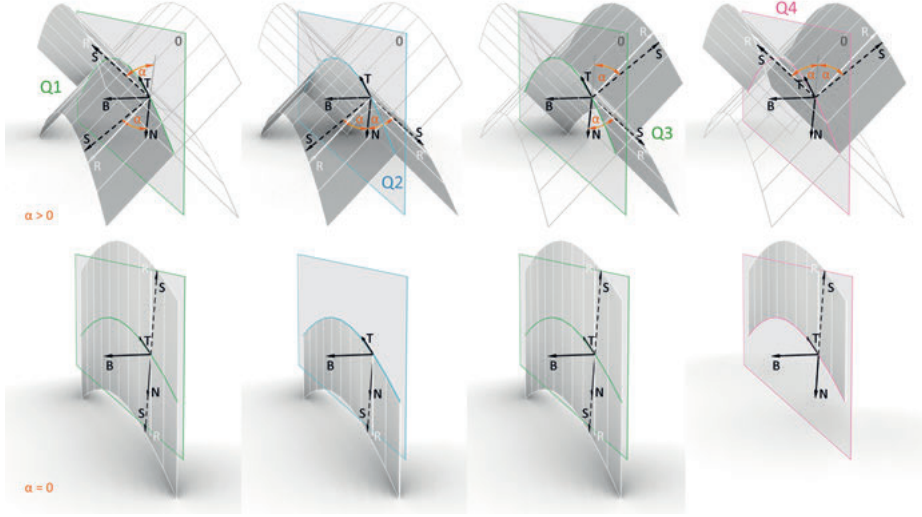
Fig. 2: Geometric principle of CCF and CCU with the concept of four quadrants. Top: actuated 3D state. Bottom: 2D crease pattern.
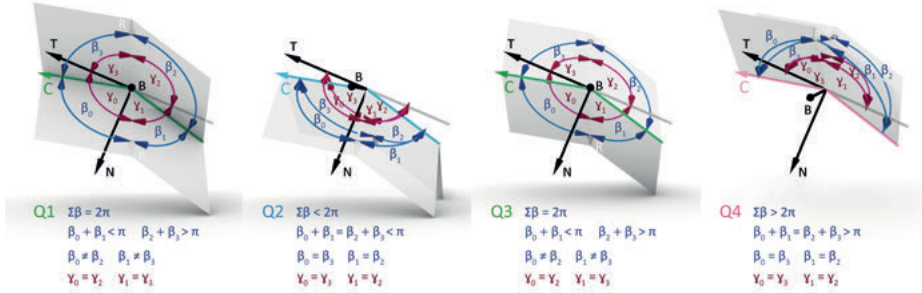

Fig. 3: Developability conditions of the four quadrants for a single vertex.

4.2 Special cases

A general crease curve possesses non-zero torsion τ and a varying reflection angle α'. These can be described for CCF with the ruling angle γ and crease curvature in the 2D pattern κ_{2D} with Eq. (1) and Eq. (3) by Fuchs and Tabachnikov (1999). The equations are adapted for CCU with Eq. (2) and Eq. (4):

$$\alpha'_{\text{CCF}} = (\cot \gamma_0 - \cot \gamma_3)\, 0.5\, \kappa_{2D} \tan \alpha \tag{1}$$

$$\alpha'_{\text{CCU}} = (\cot \gamma_0 + \cot \gamma_3)\, 0.5\, \kappa_{2D} \tan \alpha \tag{2}$$

$$\tau_{\text{CCF}} = -(\cot \gamma_0 + \cot \gamma_3)\, 0.5\, \kappa_{2D} \tan \alpha \tag{3}$$

$$\tau_{\text{CCU}} = -(\cot \gamma_0 - \cot \gamma_3)\, 0.5\, \kappa_{2D} \tan \alpha \tag{4}$$
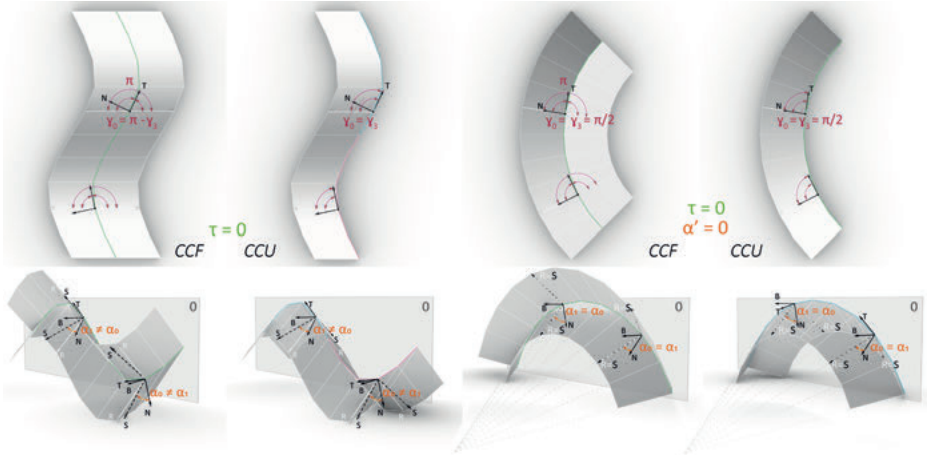
Fig. 4: The special cases of a planar crease (left), combined with a constant reflection angle (right) of CCF translated to CCU.

Special cases exist regarding crease planarity, reflection angle consistency, and a combination of both for the classic CCF (Fuchs and Tabachnikov 1999; Mundilova 2017) and are translated to CCU. In the special case of constant reflection angle $\alpha =$ const. with a non-planar crease, its change must equal $\alpha' = 0$. Hence Eq. (1) implies that, unless the crease is a straight line $\kappa_{2D} = 0$ or the system is flat $\alpha = 0$, the neighboring ruling angles across the crease must be equal in CCF, such that $\gamma_0 = \gamma_3$. This indicates that the rulings must be reflected across **T** in the 2D crease pattern, forming a kink. In CCU, the ruling is reflected across **N** in the 2D crease pattern, such that $\gamma_0 = \pi - \gamma_3$.

In the special case of a crease lying in a single osculating plane with a non-constant reflection angle, its torsion must equal $\tau = 0$. Hence Eq. (3) implies that the ruling must be reflected across **T** and **N** in CCF, such that $\gamma_0 = \pi - \gamma_3$. Consequently, the rulings are collinear in the 2D crease pattern and reflected across **O** in the 3D configuration (Fig. 4 left). In CCU, both rulings are identical, such that $\gamma_0 = \gamma_3$ or $\gamma_1 = \gamma_2$. Any developable surface type reflected at a single plane satisfies this special case. The ability of 3D reflection along a single plane permits the applicability of the reflection method.

In the ultra-special case of the combined special cases of crease planarity and constant reflection angle, both ruling conditions for CCF of their reflection across **T** $\gamma_0 = \gamma_3$ and their collinearity $\gamma_0 = \pi - \gamma_3$ must be satisfied. This implies that all ruling angles must be identical to $\gamma_0 = \gamma_3 = \pi/2$, indicating that the rulings **R** are orthogonal to **T** and coincide with the surface tangent **S** (Fig. 4 right). With the inversed equations and angle conditions, the same applies to CCU.

4.3 Deployment

The deployment mechanism is based on the equation

$$\cos \alpha = \frac{\kappa_{2D}}{\kappa_{3D}} \tag{5}$$

by Fuchs and Tabachnikov (1999). It indicates that the 3D crease curvature denoted by κ_{3D} increases proportionally to the reflection angle α during actuation. Eq. (5) holds true regardless of whether the crease is folded as CCF or CCU, as the kinematics is constrained by the planarity of a curved edge of a single developable.

In the discrete case of a mesh, the curvature κ_{2D} can be computed using the curvature radius $\mathbf{r}_{2D}$ in the direction of $\mathbf{S}$. The magnitude of $\mathbf{r}_{2D}$ can be determined with Eq. (6) using the trigonometrical relationship of the right-angled triangle formed by $\mathbf{r}_{2D}$, half of the adjacent crease edge $\mathbf{C}/2$, and the angle μ_{2D} between $\mathbf{S}$ and $\mathbf{C}$. This angle equals the average of the adjacent sector angles $\sum_{i=0}^{1} \beta_i/2$ (Fig. 5a). Similarly, the curvature κ_{3D} can be computed using the curvature radius $\mathbf{r}_{3D}$ in the direction of $\mathbf{N}$. The magnitude of $\mathbf{r}_{3D}$ can be determined with Eq. (7) using a triangle in the osculating plane $\mathbf{O}$ formed by $\mathbf{r}_{3D}$, $\mathbf{C}/2$, and the angle μ_{3D} between $\mathbf{N}$ and $\mathbf{C}$ (Fig. 5b).

$$\kappa_{2D} = \frac{1}{|\mathbf{r}_{2D}|} = \cos \mu_{2D}/(|\mathbf{C}|/2) \tag{6}$$

$$\kappa_{3D} = \frac{1}{|\mathbf{r}_{3D}|} = \cos \mu_{3D}/(|\mathbf{C}|/2) \tag{7}$$

As the crease length $|\mathbf{C}|$ remains constant during isometric transformation, Eq. (5) can be simplified for the discretized case to

$$\cos \alpha = \frac{|\mathbf{r}_{3D}|}{|\mathbf{r}_{2D}|} = \frac{\cos \mu_{2D}}{\cos \mu_{3D}} \tag{8}$$

a trigonometrical relationship of the triangle generated by $\mathbf{r}_{2D}$, $\mathbf{r}_{3D}$, which is the projection of $\mathbf{r}_{2D}$ onto $\mathbf{O}$, and the reflection angle α (Fig. 5c). Shimoda et al. (2020) derive the same cosine relationship from the length preservation specific to the ultra-special case.
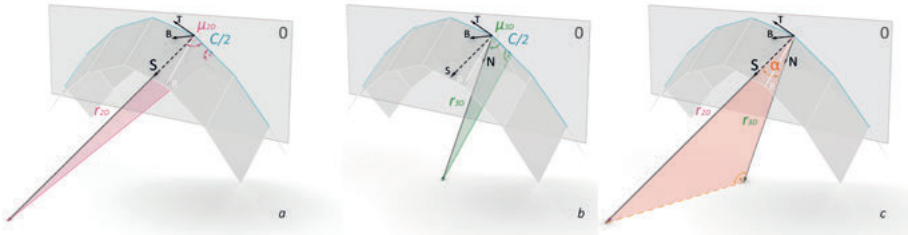

Fig. 5: Trigonometrical relationship of (a) $\mathbf{r}_{2D}$, (b) $\mathbf{r}_{3D}$, and (c) together with α.

With Eq. (8), the deployment of a crease κ_{3D} for a prescribed κ_{2D} can be simulated seamlessly for any α. Based on the trigonometric relations with γ and α, we obtain the ruling vectors **R** for the leading plate **R** = $\cos\gamma_0$ **T** + $\sin\gamma_0\cos\alpha$ **N** + $\sin\gamma_0\sin\alpha$ **B**, and the CCF plate **R**$_{CCF}$ = $\cos\gamma_3$ **T** − $\sin\gamma_3\cos\alpha$ **N** + $\sin\gamma_3\sin\alpha$ **B**, or CCU plate **R**$_{CCU}$ = $\cos\gamma_3$ **T** + $\sin\gamma_3\cos\alpha$ **N** − $\sin\gamma_3\sin\alpha$ **B**, again with inversed signs. Finally, as the isometric transformation dictates constant lengths and sector angles, the planar quad meshes are reconstructed.

5 Design rules for a multi-crease CCU system

5.1 Behavior of subsequent creases

Further plates can be constructed by trimming and reflecting the rulings at subsequent reflection planes. During deployment, the subsequent plates are reconstructed based on the leading actuated crease and the isometry constraint. However, not any subsequent plane orientation results in planar creases during the intermediate states of actuation. If both planes are parallel, they rotate with identical progression around their parallel actuation rotation axes (Fig. 6a). If one plane is inclined around the other's actuation rotation axis, both planes rotate with different progression around parallel rotation axes (Fig. 6b). In both cases, the crease curvature changes proportionally; hence the subsequent crease remains planar. However, when one plane is inclined perpendicular to the other's actuation rotation axis, the rotation axes of the planes are non-parallel (Fig. 6c). Consequently, the crease curvatures change disproportionally, and the subsequent crease does not remain on a plane (Fig. 6d). Unlike rigid origami where the rulings are fixed, the rulings can reorient during actuation in a continuously bend structures such that the CCU system can unfold nevertheless as demonstrated with FE-simulation (Fig. 6e). The system undergoes a bistable behavior as described by Rihaczek et al. (2022), with minor crease warping until the system reaches its target with planar creases.
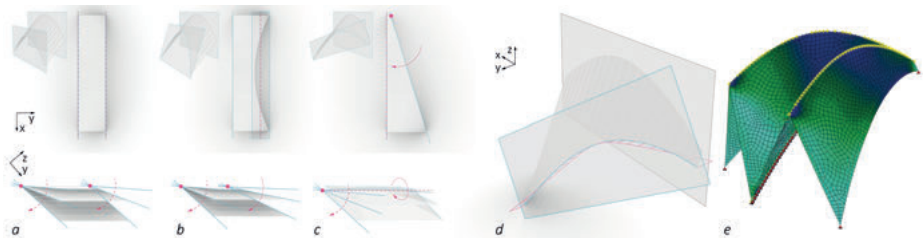

Fig. 6: Planarity of subsequent creases in relation to the osculating plane actuation rotation axes.

5.2 Translation into multi-crease corrugated structures and validation with FEA simulation

An array of parallel osculating planes generates alternating synclastic and anticlastic creases that result in a corrugated multi-crease vault structure (Fig. 1). Its geometric unfolding mechanism is verified with FEA in Fig. 7 with good congruence with deviations of 1 % of the span.

Fig. 7: FE simulation of sample from Fig. 1 (tension and compression from active bending in blue and red, respectively).

5.3 Non-zero thickness of bending-active plates

Bending-active plates require thickness for structural strength, but the induced bending stresses must respect material strength limits. This is ensured by limiting the allowable plate curvature to $\kappa_{\text{plate}} \leq f_y/(E\,0.5t)$ where f_y, E, and t denote yield strength, Young's modulus, and plate thickness (Lienhard 2014). The stresses induce positive strain $\varepsilon_+ > 0$ (red) at their extrados, negative strain $\varepsilon_- < 0$ (blue) at their intrados, while the central fiber remains neutral $\varepsilon_0 = 0$ (yellow dashed) (Fig. 8).

The bending-active plates of uniform thickness are connected using a rotation axis-shift approach (Shimoda et al. 2020). For CCF, this allows unfolding completely flat (Fig. 8a), while for the CCU, this allows folding completely closed (Fig. 8c). In CCF, an intrados connects to an extrados; thus, the strain contradicts as $\varepsilon_+ \neq \varepsilon_-$. In contrast, in the mirror-symmetric CCU, intrados connects intrados at synclastic creases and extrados to extrados at anticlastic creases; thus, the strain is compatible with $\varepsilon_+ = \varepsilon_+$ and $\varepsilon_- = \varepsilon_-$ respectively. Yet, the connection must accommodate strain as there are no one-sided-only discrete hinge zones as in rigid origami. Unlike CCF, where the rotation axes can align in one plane, either to all plates' extra- or intrados (Fig. 8b) or to the neutral fiber layer with tapering to avoid self-collision, the CCU does not allow complete closure with the volume trim method.
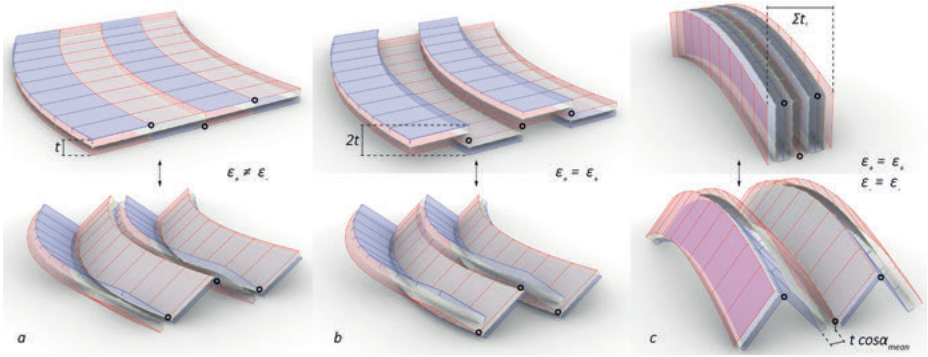
Fig. 8: Non-zero thickness (a) in CCF with axis-shift or (b) axis alignment, (c) in CCU with axis-shift.

The geometric modeling of the thickness requires offset in the vertex's normal directions by t. In the flat-folded state of CCU, the thickness equals the sum of all panels $t_{CCU} = \sum_{i=0}^{n} t$. In the actuated state, only with rulings perpendicular to the crease as in the ultra-specific case, the offset crease curve is planar (as for Shimoda et al. (2020)). Otherwise, the offset curve is corrected by intersecting the rulings with an offset plane by $\cos_{mean}$ and reversely offset to adjust the original curve.

5.4 Global shape control by variations in crease curvature

Besides the developable surface type and osculating plane layout, the global shape of a CCU structure is controlled by the profile of the crease curve, such as an arc, Elastica, catenary, funicular under asymmetric loads, and freeform curve with inflection points (Fig. 9). However, the freeform risks reaching unfolding angle limitations; ruling directions from a combination of two conical surfaces would be more suitable. The 2D crease pattern (closed-folded behind) must be computed with Eq. (8) such that it reaches its 3D target under a prescribed α (unfolded front).
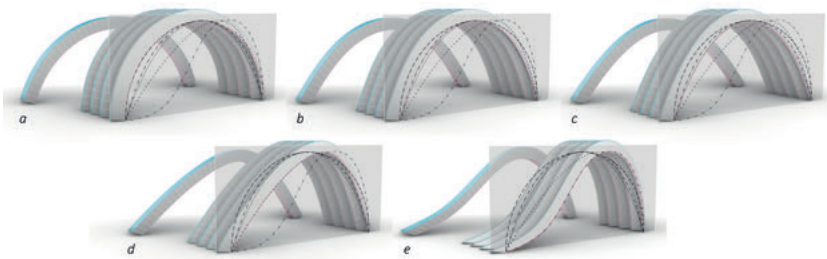

Fig. 9: Corrugated vaults with profiles of (a) arc, (b) Elastica, (c) catenary, (d) funicular with asymmetric loads, (e) freeform curve with inflection points.

5.5 Global shape control by variations in plane distance and inclinations

Even though the plates remain monoclastic throughout the isometric actuation, the multi-crease corrugated structure can be manipulated into various target global shapes through plane distance and inclination. A constant distance of parallel planes results in monoclastic vaults; decreased distance between the plates inclined towards the center generates synclastic vaults, while decreased distance between the plates inclined away from the center generates anticlastic vaults (Fig. 10). The shape is generated to fit target curves identical along the apex and supports.
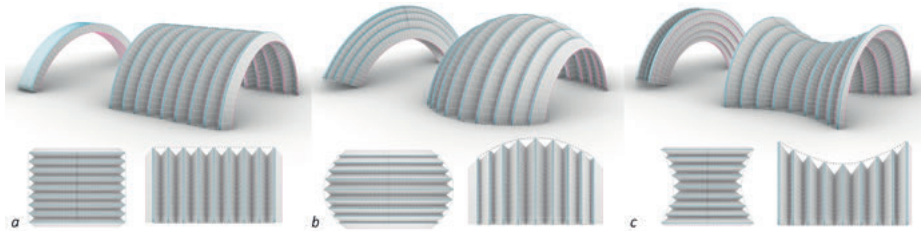

Fig. 10: Corrugated CCU vault with (a) monoclastic, (b) synclastic, (c) anticlastic curvature by plane distance solely. Top: closed and unfolded. Bottom: plan and side view.

By inclining a plane around its actuation rotation axis, the plane distance at the apex and the supports increases and decreases simultaneously. Consequently, the apex can maintain constant height while the support distance varies, and vice versa depending on plane distances, or the ridge and valley creases are articulated alternatingly at the apex and supports (Fig. 11). Furthermore, the plane inclination changes the reflected rulings' directions, resulting in variations in the corrugation depth.
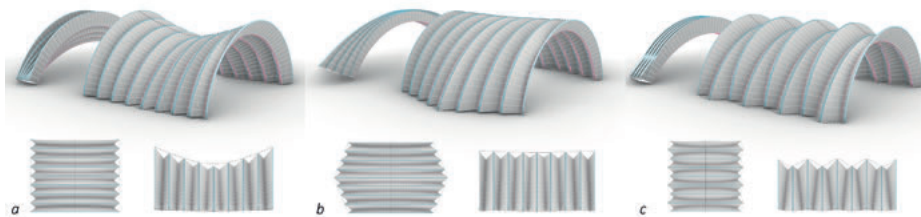

Fig. 11: Corrugated CCU vault by plane inclination around the actuation rotation axis.

By inclining a plane perpendicular to its actuation rotation axis (consider implications from Sec. 5.1), the plane distance decreases towards one end of the crease. This results

in alternating non-axisymmetric articulations to the sides (Fig. 12a). Alternatively, with consecutive inclinations in radial layouts, the structure unfolds into a corrugated dome or funnel column (Fig. 12b,c).

Fig. 12: Corrugated CCU (a) vault, (b) dome, and (c) funnel by plane inclination perpendicular to the actuation rotation axis.

6 Reflections and outlook

This research translated the geometric principles of CCF to the flat-foldable CCU system, demonstrating direct inversion in various angle correlations. It demonstrated applicability of the discrete deployment formulation and non-zero thickness with axis shift, including shape adjustment beyond the ultra-special case as in Shimoda et al. (2020). For a multi-crease system, it revealed geometric applicability of plane inclinations and demonstrated possible ruling readjustment during a bistable behavior in flexible bending-active in contrast to rigid-origami structures. This is to be further and more thoroughly investigated, but it potentially increases the design space significantly. Lastly, it demonstrated global shape control with positive and negative Gaussian curvature from developable plates and introduced a novel design language that extends the design space of CCF.

Future work will set out on design explorations of more intricate geometries and their associated formation rules by combining the control variables of crease curvature, plane distance and inclinations in both axes, by combining the CCU with CCF while avoiding self-collision, and by introducing bifurcations and non-planar creases, which will enable transitions between different types of developable surfaces and significantly expand the design space. Through feedback from funicular form-finding and FEA, the overarching objective is to obtain structurally informed structures. The numerical application developed will be distributed open-source and via an interactive Rhinoceros3D Plugin developed within the COMPAS ecosystem. Structural considerations will investigate the mechanical effect on plates and hinges and the structures' scalability potential.

Ultimately the corrugated curved plate system is to be applied on an architectural scale, materialized as a structure itself (Rihaczek et al. 2022) or as formwork for corrugated concrete shells or vaulted floors (Scheder-Bieschin et al. 2022). The bending-active plates can be materialized with plywood connected using various textile hinge strategies (Rihaczek et al. 2022; Scheder-Bieschin et al. 2022) and with GFRP connected using hinge areas of lower stiffness through fiber layout (Körner et al. 2016) or non-impregnation (Choma 2021). The crease assembly of CCU is more complex due to self-obstruction (Scheder-Bieschin et al. 2022) than the flat-assembly of CCF (Maleczek et al. 2020); however, the flat-foldable system folds more compactly than CCF. The curved-crease unfoldable bending-active system offers the advantage of a high degree of simple 2D prefabrication, flat-packed transport, and rapid on-site deployment. It results in complex, structurally-articulated 3D geometries, which would be challenging to construct otherwise and are enabled solely based on its formation principle.

References

Choma, J. 2021. Foldable composite structures. United States US10994468B2.

Fuchs, D., and S. Tabachnikov. 1999. More on Paperfolding. *The American Mathematical Monthly* 106(1): 27–35.

Körner, A., A. Mader, S. Saffarian, and J. Knippers. 2016. Bio-Inspired Kinetic Curved-Line Folding for Architectural Applications. In *ACADIA 2016,* 270–79.

Lienhard, J. 2014. Bending-Active Structures: Form-finding strategies using elastic deformation in static and kinematic systems and the structural potentials therein. Thesis, Stuttgart.

Maleczek, R., Gabriel S., A. Metzler, and C. Preisinger. 2020. Large Scale Curved Folding Mechanisms. In *DMSB 2019,* 539–53.

Mundilova, K. 2017. Geometry and Interactive Design of Curved Creases. Thesis, Wien.

Rihaczek, G., M. Klammer, O. Basnak, A. Körner, R. La Magna, and J. Knippers. 2022. Timbr Foldr: A Design Framework and Material System for Closed Cross-Section Curved Folded Structures. *JIASS* 63(4), 272–88.

Scheder-Bieschin, L., T. Van Mele, and P. Block. 2022. Curved-Crease Folding of Bending-Active Plates as Formwork: A Reusable System for Shaping Corrugated Concrete Shell Structures. In *Acadia* 2022.

Shimoda, Y., T. Tachi, and J. Sato. 2020. Flat-Foldable Rigid Origami with Uniform-Thickness Panels. In *AAG 2020.*

SOFiSTiK AG. 2022. SOFiSTiK. www.sofistik.com.

Tachi, T. 2013. Composite Rigid-Foldable Curved Origami Structure. In *First Conference Transformables 2013.*

Van Mele, T. et al. 2022. COMPAS: A Computational Framework for Collaboration and Research in Architecture, Engineering, Fabrication, and Construction. www.compas.dev